JACS
JOURNAL OF THE AMERICAN CHEMICAL SOCIETY
Article
Cite This: J. Am. Chem. Soc. XXXX, XXX, XXX−XXX
pubs.acs.org/JACS

Tipping the Balance between S-π and O-π Interactions

Jungwun Hwang,[†] Ping Li,[*,†] Mark D. Smith,[†] Constance E. Warden,[‡] Dominic A. Sirianni,[‡] Erik C. Vik,[†] Josef M. Maier,[†] Christopher J. Yehl,[†] C. David Sherrill,[‡,§] and Ken D. Shimizu[*,†]

[†]Department of Chemistry and Biochemistry, University of South Carolina, Columbia, South Carolina 29208, United States
[‡]Center for Computational Molecular Science and Technology, School of Chemistry and Biochemistry, and [§]School of Computational Science and Engineering, Georgia Institute of Technology, Atlanta, Georgia 30332, United States

Supporting Information

ABSTRACT: A comprehensive experimental survey consisting of 36 molecular balances was conducted to compare 18 pairs of S-π versus O-π interactions over a wide range of structural, geometric, and solvent parameters. A strong linear correlation was observed between the folding energies of the sulfur and oxygen balances across the entire library of balance pairs. The more stable interaction systematically switched from the O-π to S-π interaction. Computational studies of bimolecular $PhSCH_3$-arene and $PhOCH_3$-arene complexes were able to replicate the experimental trends in the molecular balances. The change in preference for the O-π to S-π interaction was due to the interplay of stabilizing (dispersion and solvophobic) and destabilizing (exchange-repulsion) terms arising from the differences in size and polarizability of the oxygen and sulfur atoms.

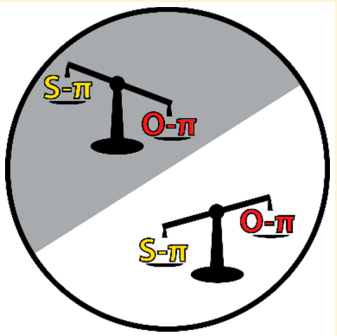

INTRODUCTION

Noncovalent interactions between sulfur atoms and aromatic surfaces are found in many biological and synthetic systems.[1−6] The attractive nature of the S-π interaction has been attributed to the enhanced dispersion[7−11] and solvophobic interactions[9,12] of the larger and more polarizable sulfur atoms. The initial evidence for the stabilizing nature of S-π interactions was the high population of sulfur-aromatic contacts in protein structure databases.[13−19] Sulfur atoms of cysteine and methionine residues are commonly found in close contact (<4.0 Å) with the aromatic faces of phenylalanine, tryptophan, or tyrosine residues.[13−16] In addition, computational studies have shown that sulfur atoms can form attractive interactions with a wide range of aromatic surfaces.[7,8,10,20−22]

However, the relative strength and importance of S-π interactions in comparison to the competing noncovalent interactions is still unclear. For example, surveys of small molecule crystallographic databases found that thioethers preferred to form close contact with the edge as opposed to the π-face of aromatic rings.[13,23] Computational studies predicted that thiols would prefer to form SH-π hydrogen bonds as opposed to S-π interactions with aromatic surfaces.[8,10,23−25] Experimental studies comparing S-π versus O-π interactions have, likewise, yielded conflicting conclusions.[12,26,27] In some cases, the S-π interactions were more stabilizing,[28−30] and in others, the O-π interactions were more stabilizing.[31−33]

Therefore, the goal of this study was to answer the question: Are S-π interactions generally more stabilizing than O-π interactions in solution? Our strategy was to experimentally measure the relative strengths of S-π versus O-π interactions across a broad series of molecular balances that vary in the interaction distance and geometry, aromatic surface size and polarity, and solvent environments. Therefore, a library of 36 small molecule model systems were prepared which provided 18 unique pairs of molecular balances that formed similar intramolecular S-π and O-π interactions (Figure 1). The diversity and size of the library provided a more comprehensive set of comparisons than previous experimental studies that primarily compared one or two pairs of structures.

RESULT AND DISCUSSION

Our *N*-phenylimide molecular balance[34,35] (Figure 1a) is a versatile model system that can accurately measure weak noncovalent interactions via their influence on the *folded*−*unfolded* equilibrium.[36] These molecular balances have been successfully applied to study many aromatic interactions including aromatic stacking,[36−39] heterocycle-π,[40] CH-π,[32,41−48] metal-π,[49] halogen-π,[50,51] and solvent effects.[46,48,52] In this study, chalcogen atoms (X = S or O) incorporated in the arm units were designed to form intramolecular chalcogen-π interactions with the π-face of the aromatic shelf in the *folded* conformers. However, in the *unfolded* conformers, the chalcogen arm and arene shelf are kept apart by the rigid bicyclic framework. Thus, variations in the strength of the intramolecular chalcogen-π interactions can be quantitatively assessed via monitoring shifts in the *folded*−*unfolded* equilibria.

A library of 36 chalcogen-π balances comprised of 18 pairs of sulfur and oxygen balances was designed to ensure that each pair formed the matching chalcogen-π interactions with the same bicyclic framework, aromatic shelf, and arm R-group

Received: July 18, 2018
Published: September 25, 2018

DOI: 10.1021/jacs.8b07617
J. Am. Chem. Soc. XXXX, XXX, XXX−XXX

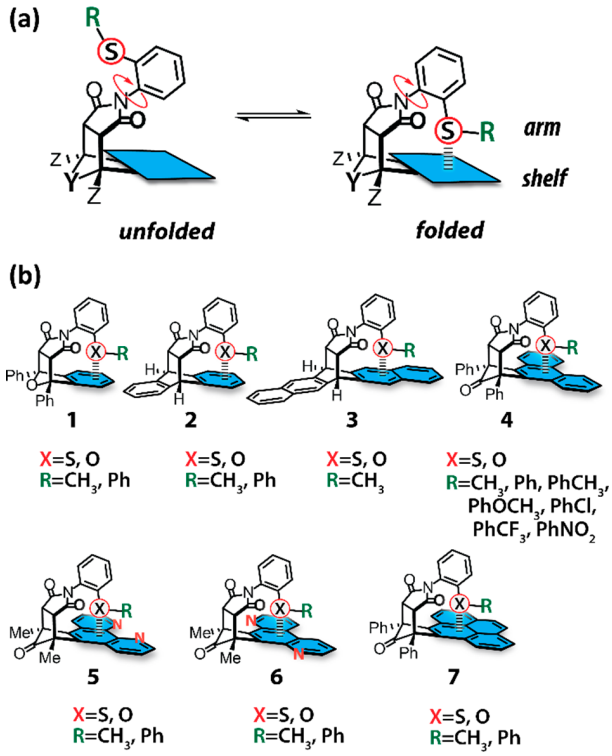

Figure 1. (a) *Folded*–*unfolded* equilibrium of the *N*-phenylimide molecular balance model that can form intramolecular S-π or O-π interaction in the *folded* conformation. (b) Chart of 36 molecular balances (18 pairs) for the comprehensive comparison of the intramolecular S-π and O-π interactions.

(Figure 1b). The balances were named using a number (**1**–**7**) corresponding to the type of bicyclic framework and aromatic shelf (Figure 1b) followed by a description of the arm unit (X-R) in parentheses. For example, balance **1(SCH$_3$)** has framework **1** with an oxygen ether bridge (Z = Ph and Y = O) and an aromatic phenylene shelf and a methyl thioether arm.

The 18 balance pairs compare S-π and O-π interactions across a wide range of structural, geometric, and solvent parameters. These include (a) the size and polarizability of the aromatic shelf, (b) the type of secondary noncovalent interactions (CH-π, aromatic stacking, and solvophobic effects) between the R-group of the arm and the aromatic shelf, (c) the geometry of chalcogen-π interaction (as modulated by the bridging Y-groups in Figure 1a),[49,53] and (d) the substituents and heteroatoms on the arm and shelf units.[40,44,51] The sulfur balances are all new compounds with the exception of **3(SMe)**, which has been previously described by Cozzi and co-workers.[32] Most of the oxygen balances have been previously employed in studies of aromatic stacking[36−39] and CH-π interactions.[41] The synthesis and characterization of all new compounds are detailed in the SI.

Characterization of S-π and O-π Interactions. The formation of intramolecular chalcogen-π interactions in the *folded* conformers was confirmed by X-ray crystallography. Crystal structures were obtained for four balance pairs (Figure 2): **3(SMe)** and **3(OMe)**, **4(SPh)$_2$** and **4(OPh)$_2$**,[36] **7(SMe)** and **7(OMe)$_2$**,[41] and **7(SPh)$_2$** and **7(OPh)$_2$**. Some balances did not crystallize in the *folded* conformation, and thus the corresponding two-armed analogs were prepared.[36,39−41,44] The two-armed balances have the identical X-R groups

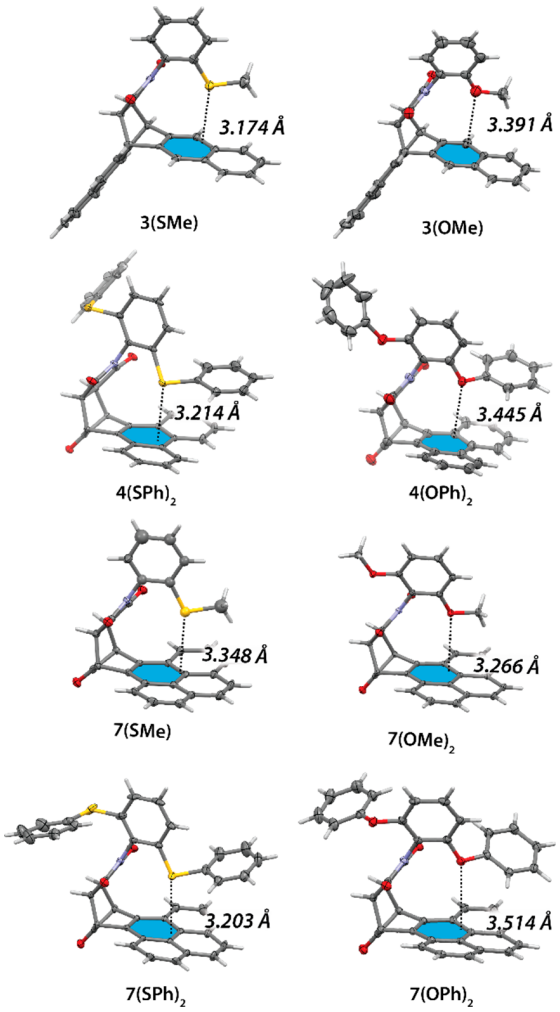

Figure 2. Side-views of eight chalcogen-π balance crystal structures: **3(SMe)**, **3(OMe)**, **4(SPh)$_2$**, **4(OPh)$_2$**, **7(SMe)**, **7(OMe)$_2$**, **7(SPh)$_2$**, and **7(OPh)$_2$**. The closest contact between the chalcogen atoms with the plane of the aromatic shelf is highlighted with a broken line. The bridgehead phenyl groups in frameworks **4** and **7** are omitted for viewing clarity.

attached at both *ortho* positions of the *N*-phenyl rotor, ensuring that one arm would always be in the *folded* geometry. The two-armed balances are denoted by a subscript 2 after the arm unit, such as **4(SPh)$_2$** and **7(OPh)$_2$**.

The expected intramolecular S-π or O-π interactions were observed in all eight balance crystal structures. The chalcogen-to-aromatic plane distances were in agreement with S-π (3.2–3.5 Å) and O-π (3.0–3.4 Å) distances from previous crystal structure surveys.[4,5] Intriguingly, the S-to-plane distances (3.17–3.27 Å) in the balance crystal structures were consistently shorter than the O-to-plane distances (3.35–3.51 Å) in all four balance pairs. This was largely due to the longer C–S (1.75–1.77 Å) versus C–O (1.34–1.38 Å) bonds that connect the arm chalcogens to the rigid bicyclic framework. The longer C–S bond positions the thioether arm closer to the aromatic shelf.

Measurement of *Folded*–*Unfolded* Equilibria. The folding energies of the 18 pairs of sulfur and oxygen balances (ΔG_S and ΔG_O) were measured in two representative organic solvents: chloroform ($CDCl_3$) and dimethyl sulfoxide (DMSO-d_6), providing 36 points of comparison. The *folded*

DOI: 10.1021/jacs.8b07617
J. Am. Chem. Soc. XXXX, XXX, XXX–XXX

and *unfolded* conformers were in slow exchange at rt due to restricted rotation of the *N*-phenyl rotors, yielding separate sets of peaks for the *folded* and *unfolded* conformers.[36] The equilibrium *folded*/*unfolded* ratios were measured by integration of the ^{1}H NMR spectra. The succinimide protons (H_a in Figure 3a) gave the most accurate integration values as they

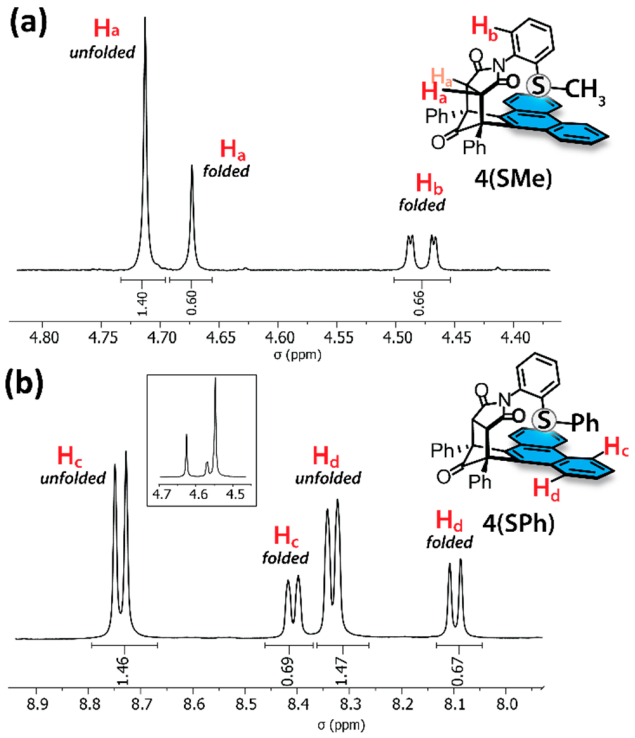

Figure 3. (a) Primary succinimide and (b) secondary aromatic peak regions of the ^{1}H NMR spectra ($CDCl_3$, 400 MHz) of **4(SMe)** and **4(SPh)**, respectively. Protons associated with the peaks are labeled in red. Inset in b show the overlapped succinimide spectral region for **4(SPh)**.

were usually distinct singlets for the two conformers. Integrations were performed using peak-fitting analysis to minimize error in the *folded*/*unfolded* ratios. The folding energies for the sulfur and oxygen balances (ΔG_S and ΔG_O) were calculated from the *folded*/*unfolded* ratios ($\Delta G = -RT \ln([folded]/[unfolded])$ and are shown in Table 1. The peaks corresponding to the *unfolded* conformer were assigned based on correlating the peak areas for the easily identifiable doublet of doublets for the *unfolded ortho* proton H_b on the *N*-phenyl rotor, which were shifted upfield to 4.0−5.0 ppm due to their position over aromatic shelf in the *unfolded* conformer. In the cases where the succinimide singlets were not well separated (Figure 3b, inset), the *folded* and *unfolded* peaks for the shelf aromatic protons (H_c and H_d in Figure 3b) were used as illustrated in the case of balance **4(SPh)** in Figure 3b. Identification of pairs of *folded* and *unfolded* peaks in the ^{1}H NMR spectra was facilitated by 2D chemical exchange NMR experiments.

Analysis of the Folding Energies for Sulfur and Oxygen Balances. To identify systematic differences in the S-π and O-π interactions in the molecular balances, the experimentally measured folding energies of the sulfur (ΔG_S) and oxygen (ΔG_O) balances of each pair were plotted against each other in a correlation plot (Figure 4). In each balance

Table 1. Folding Energies (ΔG, kcal/mol)[a] for 18 Pairs of Sulfur and Oxygen Balances in Two Solvents ($CDCl_3$ and DMSO-d_6)

	ΔG in $CDCl_3$		ΔG in DMSO-d_6	
balance	X = S	X = O	X = S	X = O
1(XMe)	2.04	1.39	1.52	0.94
1(XPh)	1.99	1.40	1.49	1.18
2(XMe)	1.11	0.78	0.75	0.54
2(XPh)	1.25	0.95	0.67	0.64
3(XMe)	0.02	0.12	−0.35	−0.09
4(XMe)	0.51	0.46	0.07	0.11
4(XPh)	0.50	0.48	0.07	0.34
4(XPhMe)	0.57	0.44	0.12	0.31
4(XPhOMe)	0.46	0.34	0.09	0.25
4(XPhCl)	0.15	0.15	−0.20	0.01
4(XPhCF$_3$)	0.09	0.12	−0.27	−0.03
4(XPhNO$_2$)	0.07	0.22	−0.43	−0.01
5(XMe)	0.27	0.22	−0.46	−0.31
5(XPh)	0.63	0.31	0.13	−0.05
6(XMe)	0.25	0.49	−0.23	−0.05
6(XPh)	−0.11	0.12	−0.50	−0.38
7(XMe)	0.14	0.22	−0.35	−0.12
7(XPh)	0.26	0.32	−0.31	−0.08

[a] ΔG values were measured at 25 °C with an error of less than ±0.03 kcal/mol. (See the SI for details of error analysis)

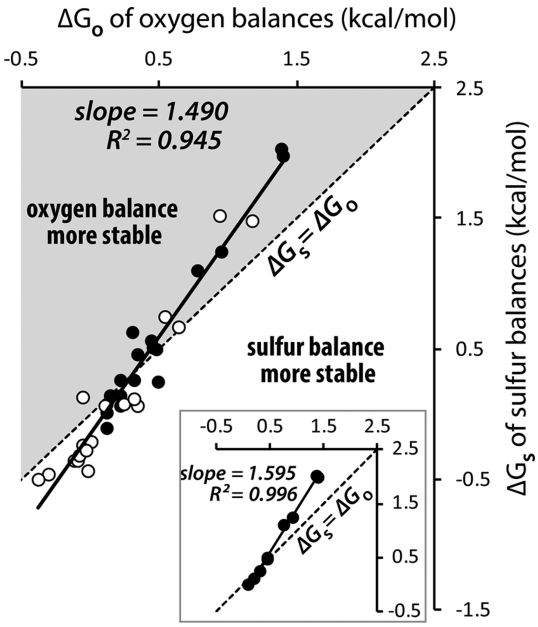

Figure 4. Correlation plot of the experimentally measured folding energies (ΔG_S and ΔG_O) for the 18 pairs of sulfur and oxygen balances in $CDCl_3$ (solid circle) and DMSO-d_6 (open circle). The broken line corresponds to the hypothetical $\Delta G_S = \Delta G_O$ line. The inset is the ΔG_S vs ΔG_O correlation plot for a subset of balance pairs lacking heteroatoms or substituents measured in $CDCl_3$: **1(XMe)**, **1(XPh)**, **2(XMe)**, **2(XPh)**, **3(XMe)**, **4(XMe)**, **4(XPh)**, **7(XMe)**, and **7(XPh)**.

pair, the framework, aromatic shelf, and arm R-group are identical. The only difference is the chalcogen atom. Thus, the correlation plot assists in isolating the differences in the S-π and O-π interactions. A strong linear correlation (R^2 = 0.945) was observed between the ΔG_S and ΔG_O values across the 18

DOI: 10.1021/jacs.8b07617
J. Am. Chem. Soc. XXXX, XXX, XXX−XXX

balance pairs and 2 solvent systems (Figure 4). A nearly perfect linear correlation was observed (R^2 = 0.996) for a more homogeneous subset of folding energies (Figure 4, inset) that were measured in $CDCl_3$ and were comprised of balance pairs lacking heteroatoms in the shelf or electron withdrawing or donating substituents in the arm unit. The strong ΔG_S versus ΔG_O correlation confirms the similarities in structures, interactions, and conformational biases between the sulfur and oxygen balances, lending support for the ability of the balance pairs to isolate and accurately compare the chalcogen-π interaction energies.

The trendline for the correlation plot also had a greater-than-unity slope (1.49), which crosses the hypothetical $\Delta G_S = \Delta G_O$ line. Thus, data points above the $\Delta G_S = \Delta G_O$ line are balance pairs where the oxygen balances have the higher *folded*/*unfolded* ratios. Data points below the $\Delta G_S = \Delta G_O$ are balance pairs where the sulfur balances have the higher *folded*/*unfolded* ratios. For example, the data point furthest above the $\Delta G_S = \Delta G_O$ line corresponds to the balance pair **1(SCH$_3$)** and **1(OCH$_3$)** measured in $CDCl_3$, where the folding energy of **1(OCH$_3$)** was 0.65 kcal/mol lower than **1(SCH$_3$)**. The point furthest below the $\Delta G_S = \Delta G_O$ line is for the balance pair **7(SPh)** and **7(OPh)** measured in DMSO-d_6, where the folding energy of **7(SPh)** was 0.21 kcal/mol lower than **7(OPh)**. This systematical switch in the folding preferences provides an explanation for the conflicting results from the previous experimental S-π versus O-π studies. The more stable chalcogen-π interaction is structure, geometry, and solvent dependent. Thus, the results from a single pairwise comparison can vary depending on where the O vs S pair falls on the energy surface.

The balance pairs favoring the O-π interaction have the lowest folding ratios and occupy the upper right quadrant of the correlation plot (Figure 4). The bias toward O-π interactions can be explained using steric repulsion arguments. Molecular modeling and X-ray crystal structure analyses concur that the rigid bicyclic framework is slightly too short.[40,41,54] Thus, the arm units (X-R) are positioned at closer-than-optimal distances from the aromatic surfaces in the *folded* conformers, and the chalcogen atoms form unfavorable steric interactions that destabilize the *folded* conformer. Balances with the smaller oxygen atoms experience weaker repulsive interactions in the *folded* conformation than those with the larger sulfur atoms.[31−33]

Despite the above-mentioned steric bias favoring the oxygen balances, approximately one-third (11 out of 36) of the balance pairs have higher folding ratios for the sulfur balances. The stabilizing S-π interactions in these balances appear to outweigh the destabilizing steric repulsion of the larger sulfur atoms. The continuity of the ΔG_S versus ΔG_O trendline suggests that these stabilizing S-π interactions are present in all pairwise comparisons. However, in many cases, the destabilizing steric repulsive interactions of the sulfur atoms outweigh the stabilizing S-π interactions.

Theoretical Comparison of S-π versus O-π Interaction. To examine the origins of the observed S-π versus O-π stability trends, computational studies were carried out. The experimental balance system is complex with many variables. The 36 pairwise comparisons of the molecular balances span multiple structural, electronic, and solvent parameters creating a complex multidimensional energy surface. In addition, the lack of crystal structures for the majority of the balances restricted the scope of structure−property analyses. Therefore, computational studies were carried out on a simple bimolecular complex comprised of an ether/thioether (Ph-X-Me, X = O or S) and a benzene ring (Figure 5a, inset). The

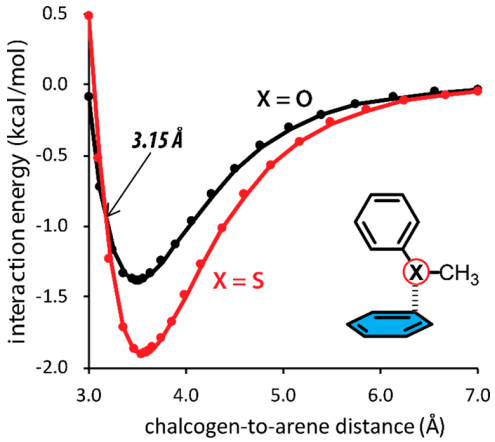

Figure 5. Calculated interaction energies (SAPT2+/aug-cc-pVDZ) for the Ph-X-CH_3···benzene (X = O or S) complexes at varying chalcogen-to-arene distances. The ether and thioethers were positioned in a similar position and geometry as the observed in the molecular balance crystal structures.

geometry of the chalcogen-π interaction in the complexes was modeled on the geometries observed in the crystal structures of the molecular balances. The ether/thioether was positioned over the π-face of the benzene ring (Figure 2) with the chalcogen atom fixed above the edge of the benzene π-face and atop one of the annular carbons. The X-CH_3 bond of the ether/thioether was held parallel to the plane of the benzene.

Each molecule of the complex was optimized separately at B3LYP/cc-pV(T+d)Z level of theory using a development version of $P_{SI}4$.[55] The molecules were frozen in their optimized geometry and positioned in the bimolecular configuration described above. Interaction energies of the ether···arene (E_O) and thioether···arene (E_S) complexes were calculated using the second-order symmetry-adapted perturbation theory method (SAPT2+/aug-cc-pVDZ).[55] Details of the computational methods are provided in the SI.

The computational study provided precise control over the variables influencing the chalcogen-π interactions. The interaction energy of the complexes was modulated by varying a single parameter D, which is the distance between the chalcogen atom and the plane of the aromatic surface (Table S14). A set of two-dimensional energy curves (Figure 5) were generated for the Ph-S-Me···benzene and Ph-O-Me···benzene complexes by varying D between 3.00 and 7.00 Å. The Ph-X-Me···benzene potential energy curves were consistent with the previous computational studies of S-π and O-π interactions.[8,9,21,56,57] For example, the thioether formed a stronger stabilizing interaction with a deeper potential energy well. The optimal distance (D_{min}) of the S-π interaction (3.6 Å) was also slightly longer in comparison to the O-π interaction (3.5 Å).

Computational analyses of the bimolecular complexes were able to reproduce the experimentally observed stability trends for the chalcogen balances. A correlation analysis (Figure 6) was carried out comparing the energy potentials of ether and thioether complexes (E_O versus E_S) at the same distances (D). The computational correlation plot was found to be linearly correlated just as the experimental correlation analysis of the

DOI: 10.1021/jacs.8b07617
J. Am. Chem. Soc. XXXX, XXX, XXX−XXX

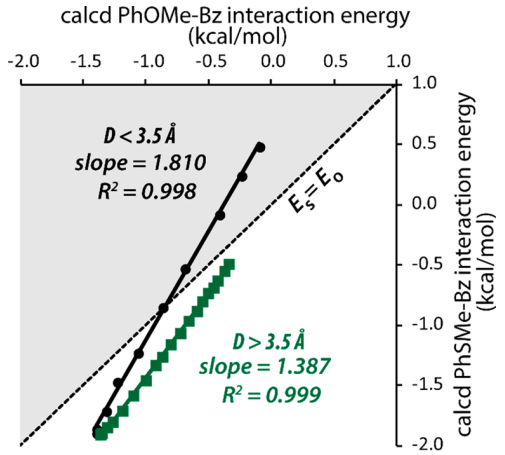

Figure 6. Correlation between the interaction energies (E_O and E_S) for the Ph-S-CH_3···benzene and Ph-O-CH_3···benzene complexes from the calculated potential curves (Figure 5). Distances shorter (D < 3.5 Å) and longer (D > 3.5 Å) than the S-π minimum are shown as black circles and green squares, respectively.

molecular balances. Interestingly, two distinct linear trendlines (green and black points) were observed in the computational study for distances on either side of the potential energy minimum (D_{min}). The segment (black points) corresponding to the distances shorter than D_{min} on the potential energy curves is more relevant to the experimental trends because of the geometry imposed by the rigid balance framework positioning the chalcogen arm in VDW contact with the aromatic shelf.[40,41,54]

The origins of the linear correlation plots were investigated by examining the components of the interaction energies: electrostatics (E_{elst}), exchange repulsion (E_{exch}), induction/polarization (E_{ind}), and London dispersion interactions (E_{disp}). These energy component terms were obtained from the SAPT2+ calculations of PhOMe···benzene and PhSMe···benzene complexes (Table S19). The difference in energy ($\Delta E = E_S - E_O$) for each term was calculated (Table 2) and plotted against the chalcogen-to-arene distance (D; Figure 7). At short distances, the difference in the total interaction

Table 2. SAPT2+ Calculated Interaction Energy Differences ($\Delta E = E_S - E_O$, kcal/mol) between the PhSMe···Benzene and PhOMe···Benzene Complexes at Varying Chalcogen-to-Arene Distances (D) from 3 to 5 Å for the Total (ΔE_{SAPT}) and Component Electrostatic (ΔE_{elst}), Exchange (ΔE_{exch}), Induction (ΔE_{ind}), and Dispersion (ΔE_{disp}) Terms

D	ΔE_{SAPT}	ΔE_{elst}	ΔE_{exch}	ΔE_{ind}	ΔE_{disp}
3.0	0.57	−3.60	7.05	−0.85	−2.04
3.1	0.16	−2.73	5.32	−0.64	−1.79
3.2	−0.13	−2.06	4.00	−0.49	−1.58
3.3	−0.32	−1.56	3.00	−0.37	−1.39
3.4	−0.44	−1.18	2.24	−0.29	−1.22
3.6	−0.54	−0.66	1.24	−0.17	−0.95
3.8	−0.52	−0.37	0.68	−0.11	−0.73
3.9	−0.49	−0.28	0.51	−0.09	−0.64
4.0	−0.46	−0.21	0.38	−0.07	−0.56
4.2	−0.38	−0.11	0.20	−0.05	−0.43
4.4	−0.31	−0.06	0.11	−0.03	−0.33
4.6	−0.25	−0.03	0.06	−0.02	−0.25
5.0	−0.15	0.00	0.02	−0.01	−0.15

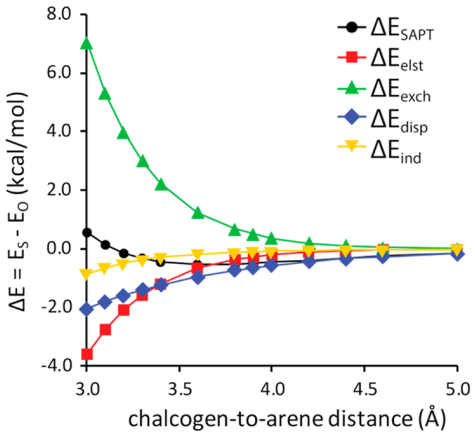

Figure 7. Energy differences ($\Delta E = E_S - E_O$, kcal/mol) between the PhSMe···benzene and PhOMe···benzene complexes for the SAPT2+ calculated energy terms (E_{elst}, E_{exch}, E_{disp}, and E_{ind}) with respect to the chalcogen-to-arene distances (D) from 3 to 5 Å.

energies (ΔE_{SAPT}) was primarily due to the destabilizing exchange-repulsion term (ΔE_{exch}) which favored the smaller oxygen atom of the ether···benzene complex. The stabilizing dispersion (ΔE_{disp}), electrostatic (ΔE_{elst}), and induction (ΔE_{ind}) terms were favorable for the PhSMe···benzene at shorter distances but were clearly overweighed by the destabilizing exchange term (ΔE_{exch}).

The switch in the more stable complex from the ether complex at shorter distances to the thioether complex at longer distances was due to the destabilizing interactions decaying more rapidly than the stabilizing interactions. The magnitude of all the contributing terms decreased with increasing distance. However, the destabilizing exchange term decayed rapidly, leaving the stabilizing electrostatic, dispersion, and induction terms dominant at longer distances. These stabilizing terms all favored the larger sulfur of the thioether···benzene complex as seen by the negative ΔE_{elst}, ΔE_{exch}, ΔE_{ind}, and ΔE_{disp} values. The favorable induction and dispersion terms are due to the larger more polarizable sulfur atoms. Interestingly, the PhSMe···benzene complex also showed a greater stabilization from the electrostatic interaction term (ΔE_{elst}) than the PhOMe···benzene complex, which is due to the enhanced orbital overlap ("charge penetration") effects for the larger sulfur atom.[58−60]

The ability of the computational study to reproduce the experimental results provides strong corroboration that the experimentally observed stability trends are due to the intrinsic differences in the S-π versus O-π interactions. The computational and experimental model systems differ significantly in nature of the interaction (intermolecular versus intramolecular), environment (vacuum versus solution), and methods of modulating the interaction energy (multiple parameters versus distance). The linear correlation and the switch in the preference in stability were also computationally observed for other geometries (Figure S1) and for larger aromatic surfaces such as naphthalene (Figure S2). This provides further support for the generality of the computationally and experimentally observed S-π and O-π trends.

The computational study yielded insights into the origins of the S-π versus O-π trends. First, the switch in the S-π versus O-π stability trends is due to the balance of the attractive and repulsive interactions of the larger sulfur atom. The interaction energy of the thioether···arene complex is stronger than the

DOI: 10.1021/jacs.8b07617
J. Am. Chem. Soc. XXXX, XXX, XXX−XXX

ether···arene complex at distances close to the minimum (D_{min}) and longer due to the deeper potential of the S-π interaction. This is primarily due to the stronger dispersion interactions of the larger and more polarizable sulfur atoms. The attractive electrostatic and induction interactions also favor the S-π interactions but to a lesser extent. A reversal of selectivity is observed at shorter distances due to the dominance of the repulsive exchange interactions, which favor the smaller oxygen atoms. This results in the ether··· arene complex becoming the more stable complex at shorter distances.

The SAPT analysis also provided an explanation for the linear correlation between the S-π versus O-π interaction energies. The ratio of the contributing energy terms for the thioether and ether complexes (E_S/E_O) is constant over a wide range of distances (Table S19). For example, the ratios of the two most dominant energy components, E_{exch} and E_{disp}, fell within a narrow range between 1.6 and 1.7 and 1.2−1.3, respectively, for all distances between 3 and 5 Å. The exchange term is dominant at shorter distances, and the dispersion term is dominant at longer distances. Thus, the correlation plot for the SAPT interaction energies of the thioether and ether complexes have distinct linear regions for the distances less than ($<D_{min}$) or greater than ($>D_{min}$) the optimal interaction distance (Figure 6). The ratios of the energy components are considered to arise from the intrinsic difference between sulfur and oxygen atoms and appear to be constant not only along the distance variable but also across other variables such as geometry, solvent, and structure, which is evidenced by the strong linear correlation observed in the multivariable experimental molecular balance study.

CONCLUSION

In conclusion, we synthesized and measured a large library of chalcogen-π molecular balances to comprehensively compare the S-π and O-π interactions. The 18 balance pairs varying in their geometry, structure, and supporting interactions were measured in two different solvents (DMSO and chloroform) providing 36 unique points of comparison. A linear correlation was observed between the folding energies of the matching sulfur and oxygen balances, suggesting that the balance frameworks in each pair are sufficiently similar to allow for accurate isolation and comparison of the S-π and O-π interactions. Interestingly, the linear correlation with a larger-than-unity slope systematically switched the stability preference from the O-π interaction in the less *folded* balances to the S-π interaction in the more *folded* balances. Computational studies comparing bimolecular ether···arene and thioether··· arene complexes were able to reproduce both the linear correlation between S-π and O-π interaction energies and the systematic switch in the more stable interaction from O-π to S-π. The energy surfaces in the bimolecular complexes were explored by systematically varying the chalcogen-to-arene distance, which was very different from the multiple parameters varied in the experimental study and, yet, still yielded similar stability trends. The linear correlation between the chalcogen-π interaction energies appears to be due to the similar shape of the chalcogen-π potential curves. The switch in more stable chalcogen-π interaction appears to be due to the deeper energy minimum of the S-π interaction at optimal distances, where the S-π interaction is the more stable. But the S-π interaction displays stronger exchange-repulsion at shorter distances, which leads to the O-π interaction becoming more stable. SAPT analysis confirmed the interplay between the greater destabilizing exchange-repulsion and stabilizing dispersion interactions of the larger and more polarizable sulfur atom varies with the distance of the chalcogen from the arene surface.

ASSOCIATED CONTENT

Supporting Information

The Supporting Information is available free of charge on the ACS Publications website at DOI: 10.1021/jacs.8b07617.

Additional data on the compounds studied (CIF)
Additional tables and figures, details on the preparation of the molecular balances, measurement of folded/unfolded ratios, error analysis, characterization of the S-π and O-π interactions in crystal structures, crystal structures, theoretical calculations, ^{1}H and ^{13}C NMR spectra (PDF)

AUTHOR INFORMATION

Corresponding Authors

*li246@mailbox.sc.edu
*shimizu@mail.chem.sc.edu

ORCID

Ping Li: 0000-0001-9339-3111
Dominic A. Sirianni: 0000-0002-6464-0213
C. David Sherrill: 0000-0002-5570-7666
Ken D. Shimizu: 0000-0002-0229-6541

Notes

The authors declare no competing financial interest.

ACKNOWLEDGMENTS

Funding for this work was provided by the National Science Foundation Grants CHE 1709086, CHE 1310139, and CHE 1566192.

REFERENCES

(1) Lewis, A. K.; Dunleavy, K. M.; Senkow, T. L.; Her, C.; Horn, B. T.; Jersett, M. A.; Mahling, R.; McCarthy, M. R.; Perell, G. T.; Valley, C. C.; Karim, C. B.; Gao, J. L.; Pomerantz, W. C. K.; Thomas, D. D.; Cembran, A.; Hinderliter, A.; Sachs, J. N. *Nat. Chem. Biol.* **2016**, *12* (10), 860−866.
(2) Beno, B. R.; Yeung, K. S.; Bartberger, M. D.; Pennington, L. D.; Meanwell, N. A. *J. Med. Chem.* **2015**, *58* (11), 4383−4438.
(3) Daeffler, K. N. M.; Lester, H. A.; Dougherty, D. A. *J. Am. Chem. Soc.* **2012**, *134* (36), 14890−14896.
(4) Salonen, L. M.; Ellermann, M.; Diederich, F. *Angew. Chem., Int. Ed.* **2011**, *50* (21), 4808−4842.
(5) Mooibroek, T. J.; Gamez, P.; Reedijk, J. *CrystEngComm* **2008**, *10* (11), 1501−1515.
(6) Aledo, J. C.; Canton, F. R.; Veredas, F. J. *Sci. Rep.* **2015**, *5*, 16955.
(7) Duan, G. L.; Smith, V. H.; Weaver, D. F. *Mol. Phys.* **2001**, *99* (19), 1689−1699.
(8) Ringer, A. L.; Senenko, A.; Sherrill, C. D. *Protein Sci.* **2007**, *16* (10), 2216−2223.
(9) Valley, C. C.; Cembran, A.; Perlmutter, J. D.; Lewis, A. K.; Labello, N. P.; Gao, J.; Sachs, J. N. *J. Biol. Chem.* **2012**, *287* (42), 34979−34991.
(10) Tauer, T. P.; Derrick, M. E.; Sherrill, C. D. *J. Phys. Chem. A* **2005**, *109* (1), 191−196.
(11) Morgado, C. A.; McNamara, J. P.; Hillier, I. H.; Burton, N. A. *J. Chem. Theory Comput.* **2007**, *3* (5), 1656−1664.
(12) Tatko, C. D.; Waters, M. L. *Protein Sci.* **2004**, *13* (9), 2515−2522.

DOI: 10.1021/jacs.8b07617
J. Am. Chem. Soc. XXXX, XXX, XXX−XXX

(13) Zauhar, R. J.; Colbert, C. L.; Morgan, R. S.; Welsh, W. J. *Biopolymers* **2000**, *53* (3), 233−248.
(14) Warme, P. K.; Morgan, R. S. *J. Mol. Biol.* **1978**, *118* (3), 289−304.
(15) Reid, K. S. C.; Lindley, P. F.; Thornton, J. M. *FEBS Lett.* **1985**, *190* (2), 209−213.
(16) Hussain, H. B.; Wilson, K. A.; Wetmore, S. D. *Aust. J. Chem.* **2015**, *68* (3), 385−395.
(17) Chakrabarti, P.; Bhattacharyya, R. *Prog. Biophys. Mol. Biol.* **2007**, *95* (1−3), 83−137.
(18) Bhattacharyya, R.; Pal, D.; Chakrabarti, P. *Protein Eng., Des. Sel.* **2004**, *17* (11), 795−808.
(19) Pal, D.; Chakrabarti, P. *J. Biomol. Struct. Dyn.* **2001**, *19* (1), 115−128.
(20) Cabaleiro-Lago, E. M.; Rodriguez-Otero, J.; Pena-Gallego, A. *J. Chem. Phys.* **2008**, *129* (8), 084305.
(21) Gomez-Tamayo, J. C.; Cordomi, A.; Olivella, M.; Mayol, E.; Fourmy, D.; Pardo, L. *Protein Sci.* **2016**, *25* (8), 1517−1524.
(22) Sencanski, M.; Dosen-Micovic, L.; Sukalovic, V.; Kostic-Rajacic, S. *Struct. Chem.* **2015**, *26* (4), 1139−1149.
(23) Forbes, C. R.; Sinha, S. K.; Ganguly, H. K.; Bai, S.; Yap, G. P. A.; Patel, S.; Zondlo, N. J. *J. Am. Chem. Soc.* **2017**, *139* (5), 1842−1855.
(24) Biswal, H. S.; Wategaonkar, S. *J. Phys. Chem. A* **2009**, *113* (46), 12774−12782.
(25) Alberti, M.; Aguilar, A.; Huarte-Larranaga, F.; Lucas, J. M.; Pirani, F. *J. Phys. Chem. A* **2014**, *118* (9), 1651−1662.
(26) Viguera, A. R.; Serrano, L. *Biochemistry* **1995**, *34* (27), 8771−8779.
(27) Motherwell, W. B.; Moreno, R. B.; Pavlakos, I.; Arendorf, J. R. T.; Arif, T.; Tizzard, G. J.; Coles, S. J.; Aliev, A. E. *Angew. Chem., Int. Ed.* **2018**, *57* (5), 1193−1198.
(28) Liu, T.; Schneider, H.-J. *Angew. Chem., Int. Ed.* **2002**, *41* (8), 1368−1370.
(29) Breinlinger, E. C.; Keenan, C. J.; Rotello, V. M. *J. Am. Chem. Soc.* **1998**, *120* (34), 8606−8609.
(30) Motherwell, W. B.; Moise, J.; Aliev, A. E.; Nic, M.; Coles, S. J.; Horton, P. N.; Hursthouse, M. B.; Chessari, G.; Hunter, C. A.; Vinter, J. G. *Angew. Chem., Int. Ed.* **2007**, *46* (41), 7823−7826.
(31) Zoltewicz, J. A.; Lavieri, S. *J. Org. Chem.* **2001**, *66* (21), 7227−7230.
(32) Raimondi, L.; Benaglia, M.; Cozzi, F. *Eur. J. Org. Chem.* **2014**, *23*, 4993−4998.
(33) Benaglia, M.; Cozzi, F.; Mancinelli, M.; Mazzanti, A. *Chem. - Eur. J.* **2010**, *16* (25), 7456−7468.
(34) Paliwal, S.; Geib, S.; Wilcox, C. S. *J. Am. Chem. Soc.* **1994**, *116* (10), 4497−4498.
(35) Mati, I. K.; Cockroft, S. L. *Chem. Soc. Rev.* **2010**, *39* (11), 4195−4205.
(36) Carroll, W. R.; Pellechia, P.; Shimizu, K. D. *Org. Lett.* **2008**, *10* (16), 3547−3550.
(37) Hwang, J.; Li, P.; Carroll, W. R.; Smith, M. D.; Pellechia, P. J.; Shimizu, K. D. *J. Am. Chem. Soc.* **2014**, *136* (40), 14060−14067.
(38) Hwang, J.; Dial, B. E.; Li, P.; Kozik, M. E.; Smith, M. D.; Shimizu, K. D. *Chem. Sci.* **2015**, *6* (7), 4358−4364.
(39) Hwang, J.; Li, P.; Smith, M. D.; Shimizu, K. D. *Angew. Chem., Int. Ed.* **2016**, *55* (28), 8086−8089.
(40) Li, P.; Zhao, C.; Smith, M. D.; Shimizu, K. D. *J. Org. Chem.* **2013**, *78* (11), 5303−5313.
(41) Carroll, W. R.; Zhao, C.; Smith, M. D.; Pellechia, P. J.; Shimizu, K. D. *Org. Lett.* **2011**, *13* (16), 4320−4323.
(42) Zhao, C.; Parrish, R. M.; Smith, M. D.; Pellechia, P. J.; Sherrill, C. D.; Shimizu, K. D. *J. Am. Chem. Soc.* **2012**, *134* (35), 14306−14309.
(43) Zhao, C.; Li, P.; Smith, M. D.; Pellechia, P. J.; Shimizu, K. D. *Org. Lett.* **2014**, *16* (13), 3520−3523.
(44) Li, P.; Parker, T. M.; Hwang, J.; Deng, F.; Smith, M. D.; Pellechia, P. J.; Sherrill, C. D.; Shimizu, K. D. *Org. Lett.* **2014**, *16* (19), 5064−5067.
(45) Li, P.; Hwang, J.; Maier, J. M.; Zhao, C.; Kaborda, D. V.; Smith, M. D.; Pellechia, P. J.; Shimizu, K. D. *Cryst. Growth Des.* **2015**, *15* (8), 3561−3564.
(46) Maier, J. M.; Li, P.; Vik, E. C.; Yehl, C. J.; Strickland, S. M. S.; Shimizu, K. D. *J. Am. Chem. Soc.* **2017**, *139* (19), 6550−6553.
(47) Emenike, B. U.; Bey, S. N.; Bigelow, B. C.; Chakravartula, S. V. S. *Chem. Sci.* **2016**, *7* (2), 1401−1407.
(48) Emenike, B. U.; Bey, S. N.; Spinelle, R. A.; Jones, J. T.; Yoo, B.; Zeller, M. *Phys. Chem. Chem. Phys.* **2016**, *18* (45), 30940−30945.
(49) Maier, J. M.; Li, P.; Hwang, J.; Smith, M. D.; Shimizu, K. D. *J. Am. Chem. Soc.* **2015**, *137* (25), 8014−8017.
(50) Sun, H.; Horatscheck, A.; Martos, V.; Bartetzko, M.; Uhrig, U.; Lentz, D.; Schmieder, P.; Nazare, M. *Angew. Chem., Int. Ed.* **2017**, *56* (23), 6454−6458.
(51) Li, P.; Maier, J. M.; Vik, E. C.; Yehl, C. J.; Dial, B. E.; Rickher, A. E.; Smith, M. D.; Pellechia, P. J.; Shimizu, K. D. *Angew. Chem., Int. Ed.* **2017**, *56* (25), 7209−7212.
(52) Maier, J. M.; Li, P.; Ritchey, J. S.; Yehl, C. J.; Shimizu, K. D. *Chem. Commun.* **2018**, *54*, 8502−8505.
(53) Bhayana, B.; Ams, M. R. *J. Org. Chem.* **2011**, *76* (9), 3594−3596.
(54) Nijamudheen, A.; Jose, D.; Shine, A.; Datta, A. *J. Phys. Chem. Lett.* **2012**, *3* (11), 1493−1496.
(55) Parrish, R. M.; Burns, L. A.; Smith, D. G. A.; Simmonett, A. C.; DePrince, A. E.; Hohenstein, E. G.; Bozkaya, U.; Sokolov, A. Y.; Di Remigio, R.; Richard, R. M.; Gonthier, J. F.; James, A. M.; McAlexander, H. R.; Kumar, A.; Saitow, M.; Wang, X.; Pritchard, B. P.; Prakash, V.; Schaefer, H. F.; Patkowski, K.; King, R. A.; Valeev, E. F.; Evangelista, F. A.; Turney, J. M.; Crawford, T. D.; Sherrill, D. *J. Chem. Theory Comput.* **2017**, *13* (7), 3185−3197.
(56) Amicangelo, J. C.; Gung, B. W.; Irwin, D. G.; Romano, N. C. *Phys. Chem. Chem. Phys.* **2008**, *10* (19), 2695−2705.
(57) Ran, J.; Hobza, P. *J. Chem. Theory Comput.* **2009**, *5* (4), 1180−1185.
(58) Stone, A. J. *The Theory of Intermolecular Forces*; Oxford University Press: Oxford, U.K., 1996.
(59) Parker, T. M.; Hohenstein, E. G.; Parrish, R. M.; Hud, N. V.; Sherrill, C. D. *J. Am. Chem. Soc.* **2013**, *135* (4), 1306−1316.
(60) Hohenstein, E. G.; Duan, J. N.; Sherrill, C. D. *J. Am. Chem. Soc.* **2011**, *133* (34), 13244−13247.

DOI: 10.1021/jacs.8b07617
J. Am. Chem. Soc. XXXX, XXX, XXX−XXX